energies

Article

Enhancing Resilience and Reliability of Active Distribution Networks through Accurate Fault Location and Novel Pilot Protection Method

Lin Xu [1], Songhai Fan [1], Hua Zhang [1], Jiayu Xiong [1], Chang Liu [1] and Site Mo [2,*]

[1] Electric Power Research Institute, State Grid Sichuan Electric Power Company, Chengdu 610095, China; 15208137140@163.com (L.X.); fansonghai@126.com (S.F.); hz1136560400@126.com (H.Z.); zelosxiong@hotmail.com (J.X.); cl2286104712@163.com (C.L.)
[2] College of Electrical Engineering, Sichuan University, Chengdu 610065, China
* Correspondence: mosite@126.com

Abstract: The integration of distributed generation (DG) into the decentralized access of the distribution network transforms the existing structure into an active distribution network. The alteration in fault characteristics poses significant challenges to the coordinated operation of relay protection. Fault location within the distribution network plays a vital role in facilitating fault recovery and enhancing the resilience of the power system. It proves instrumental in improving the network's ability to withstand extreme disasters, thereby enhancing the reliability of power distribution. Therefore, this paper provides a detailed analysis of the voltage fault components occurring during various fault types within an active distribution network. Building upon the identified characteristics of voltage fault components, a novel approach for the longitudinal protection of active distribution networks is proposed. This method involves comparing the calculated values of voltage fault components with their actual values. The proposed approach is applicable to various fault scenarios, including short-circuit faults, line break faults, and recurring faults. It exhibits advantages such as insensitivity to the penetration of distributed power supplies and robustness in withstanding transition resistance. The simulation results validate the effectiveness of the proposed method, affirming its applicability to diverse protection requirements within active distribution networks.

Keywords: active distribution network; short-circuit fault; line break fault; fault location; pilot protection

check for updates

Citation: Xu, L.; Fan, S.; Zhang, H.; Xiong, J.; Liu, C.; Mo, S. Enhancing Resilience and Reliability of Active Distribution Networks through Accurate Fault Location and Novel Pilot Protection Method. *Energies* **2023**, *16*, 7547. https://doi.org/10.3390/en16227547

Academic Editor: Javier Contreras

Received: 15 October 2023
Revised: 27 October 2023
Accepted: 1 November 2023
Published: 13 November 2023

1. Introduction

The increasing demands for reliability in distribution networks align with the ongoing development of society. Under normal operating conditions, distribution networks can swiftly identify fault components, isolate faults, and restore power supplies [1,2]. Nevertheless, in recent years, the occurrence of high-impact and low-probability (HILP) events has increased, resulting in catastrophic failures in power systems [3]. These events adversely affect numerous power components, thereby severely compromising the safe and reliable operation of distribution networks. The occurrence of power outages due to disasters, both domestically and internationally, has emphasized the urgent necessity to enhance the reliability of power grids [4,5]. For example, in September 2016, severe storms and lightning struck Australia, causing overnight power losses for 1.6 million residents in South Australia [6]. Similarly, in February 2021, Texas faced a cold wave of ice and snow, compelling the shutdown of 40,000 MW generating units. The maximum power limit load exceeded 20% of the pre-incident load, leaving approximately 5 million users without power [7].

Catastrophic failures resulting from extreme disasters continue to pose significant threats to the uninterrupted and stable power supply provided by distribution networks. To evaluate the power system's ability to withstand extreme disasters and recover from fault states, scholars have introduced the concept of 'resilience' [8,9]. Resilience encompasses not only the system's capacity to enhance its ability to recover but also emphasizes the system's reliable absorption and adaptation to external disturbances. This enables it to maintain operational functionality to the greatest extent possible and promptly return to normal operation [10]. In the event of a fault in the distribution network, a highly resilient distribution network can not only swiftly prevent fault propagation and facilitate fault removal but also expeditiously restore normal and stable operational states. This ensures the reliability of the power supply within the distribution network [11,12].

Active distribution networks (ADNs) play a crucial role in the integration of large-scale intermittent renewable energy sources and in enhancing the reliability of users' power consumption [13]. It is evident that ADNs will shape the future development of distribution networks. Compared to transmission networks, distribution networks have lower redundancy, aging equipment, outdated protection methodologies, and limited resilience against extreme disasters [14,15]. Consequently, distribution networks are significantly impacted by extreme disasters. In such scenarios, fast and accurate fault localization becomes a prerequisite for enhancing the resilience and power supply reliability of distribution networks [16].

Considerable research has been conducted by many scholars on active distribution network protection. Table 1 provides a horizontal comparison between the method proposed in this paper and other existing methods. The comparison indicates that the proposed method exhibits strong functionality and adaptability, enabling the identification of short-circuit and open-circuit faults even in scenarios with high fault resistance and penetration rates. Existing protection schemes for distribution networks can be categorized as follows:

1. Enhancement of Traditional Current Protection and Distance Protection: Traditional current and distance protection methods have been improved to accommodate the integration of distributed generation. Proposed adaptations include adaptive current protection or combinations with other protection methods. While directional current protection can adapt to power flow changes resulting from DG integration, traditional directional overcurrent protection schemes suffer from lengthy operation times. To address this, a directional overcurrent protection scheme utilizing double renormalization was proposed in [17] using double renormalization. Each protection setting included two inverse-time overcurrent protection settings based on fault direction.

In [18], a distance protection scheme suitable for highly permeable active distribution networks was proposed. Compared to traditional distance protection, this approach incorporated additional parameters, such as distribution transformer parameters and upstream system zero-sequence impedance, effectively enhancing protection performance. A novel directional relay protection scheme based on post-fault current was introduced in [19]. By defining a new fault current vector, this scheme succeeded in detecting power direction and determining fault location solely based on post-fault current, independent of power direction, fault transition resistance, and fault starting angle. This method, relying solely on local information, reduced the dependence on communication, enabling easy implementation and rapid response.

However, due to its reliance on local information, this approach faces challenges in fully adapting to the complex fault conditions in distribution networks. This is particularly true with the increasing penetration of distributed power sources and the influence of extreme disasters. Consequently, there is a need to further enhance active distribution network protection schemes;

2. Centralized Protection Scheme: The centralized protection scheme utilizes multi-point information, where measurement information from various points is transmitted to the distribution terminal. The master station utilizes this multi-point measurement information to identify the fault area [5].

In [20], a centralized intelligent protection scheme based on communication was proposed, and the communication model and hardware architecture of the protection scheme were given. The protection scheme employed various protection criteria to guarantee protection selectivity. In [21], an intelligent protection scheme for complex distribution networks based on the wireless token ring protocol (WTRP) was introduced. By leveraging a wireless token ring network protocol for relay data sharing, stations no longer require direct connections to each other or to the main station. This approach effectively enhanced the accuracy and reliability of distribution network protection.

Compared to local protection that uses local information, centralized protection using multi-point information can adapt to complex distribution network faults, leading to more accurate fault identification. However, centralized protection often relies on the availability of multi-point information, demanding high communication and data processing capabilities at the master station. Additionally, because the centralized protection scheme relies on the master station for decision making, it becomes vulnerable to failure in the event of communication or a master station malfunction;

3. Based on the pilot protection of communication: A pilot protection can be constructed using various fault characteristics such as phase current amplitude, current fault component amplitude, and current phase angle change direction.

In [22], an active distribution network protection scheme was proposed using the positive sequence current mutation at both ends of the line. The protection scheme represents the positive sequence current mutation in the form of a binary to extract the current direction information. This information acquisition method is simple and has low requirements for data communication synchronization. In addition, the scheme has good anti-interference to harmonics, noise, and measurement errors generated using power electronic devices, nonlinear loads, and switching operations. To enhance protection sensitivity and mitigate the influence of load, a new longitudinal current differential protection scheme was constructed. This scheme, detailed in [23], utilizes the positive sequence fault component. The realization of the scheme involved the utilization of both the data synchronization scheme and point-to-point communication technology. In addition, a protection prototype was developed to test the proposed method.

The pilot protection can accurately identify the fault in the feeder area only by using the information on both sides of the line. It has the advantages of both centralized protection and local protection. It can reflect any point fault in the line area and has absolute selectivity [24]. At present, many scholars have studied the pilot protection of active distribution networks;

4. Protection against line break faults: The treatment of short-circuit faults in distribution networks has received substantial attention in current research. However, studies addressing line break faults remain limited. Most research focused on fault detection and fault section location in traditional distribution networks, identifying faults by analyzing the voltage at both ends of the line.

In [25], an analysis was conducted on the voltage characteristics of various types of single-phase line break faults in resonant grounding systems. Considering factors such as fault point location, unbalanced load impedance, and grounding resistance, a detailed mathematical model was established. This model enables accurate identification of single-phase line break faults and single-phase grounding faults.

In [26], a technique was introduced to differentiate between line break faults and medium-voltage side short-circuit faults. This method involved analyzing the voltage amplitude and phase on the low-voltage side of the distribution transformer (DT) using the symmetrical component method. The amplitude was used to distinguish two-phase faults with line breaks (TPFs-LBs) and two-phase short-circuit faults (TPFs-SCs). The phase was used to distinguish single-line-to-ground faults with line breaks (SLGFs-LBs) and single-line-to-ground faults (SLGFs). This method demonstrated robustness under extreme operating conditions, considering different network topologies and radial distribution networks.

Table 1. Comparison between different fault location methods.

Ref.	Techniques	Equipment [1]	Measured Parameters	Fault Types [2]	Results [3]	Contributions
[27]	Improved current protection and distance protection	Distance relay, PT, CT, Phase selector	Current and voltage phasor	1ph-g, 3p, 2ph-g, 2p	Fault distance, fault type, fault phase	Strong adaptability to fault resistance and system operating conditions
[28]		Relay, PT, CT, Circuit breaker	Current and voltage phasor	1ph-g, 2ph-g	Fault distance	Simple calculation and not affected by fault resistance
[20]	Centralized protection	Relay, CIU, VIU, BIU, VT, CPU, CB, Directional element	Current and voltage magnitude	2p	Fault section, fault region, fault type	Fast fault clearing time; high reliability and suitable for high permeability network
[29]		Relay, IED	Current magnitude	Pole-to-ground fault	Fault section, fault region	High adaptability to communication delay, communication failure, and fault resistance
[22]	Pilot protection	Relay, Communication system	Current phasor	1ph-g, 3p, 2p	Fault section	Low requirements for data communication and great anti-interference to different reactive currents and load switching
[23]		STU, WLAN	Current phasor	2p, 3p	Fault region, fault section	Does not depend on communication channel or external GPS clock; high reliability
[30]	Line break fault protection	PMU, Wireless communication	Voltage phasor	SLGF-LB, 1ph-g	Distinguishing 1ph g and SLGF-LB	Keeping high accuracy and robustness even in extreme cases, such as frequency fluctuation and power factor
[26]		TTU	Voltage phasor	SLGF-LB, 1ph-g, TPF-LB, 2p	Distinguishing 1ph-g, SLGF-LB, TPF-LB, and 2p	Effective and robust in different topologies and under extreme cases of radial distribution networks
[31]	Elastic mapping	PMU at bifurcations	Voltage phasor	All types	Fault region, fault severity	Proposed a distribution network fault location and severity assessment method with 99% accuracy

Table 1. *Cont.*

Ref.	Techniques	Equipment [1]	Measured Parameters	Fault Types [2]	Results [3]	Contributions
This paper	Pilot protection	PMU	Current and voltage magnitude	All types (including line break fault and multiple fault)	Fault region, fault section	Short-circuit and line break faults can be detected; high adaptability to fault resistance and high permeability network

[1] PT: potential transformer; CT: current transformer; CIU: current interface unit; VIU: voltage interface unit; BIU: circuit breaker interface units; CB: circuit breaker; CPU: central protection unit; PMU: phasor measurement unit; LAN: local area network; IED: intelligent electronic devices; TTU: transformer supervisory terminal units; WLAN: wireless local area network; and STU: smart terminal unit. [2] 1ph-g: one-phase ground fault; 2p: two-phase short-circuit faults; 2ph-g: two-phase ground faults; and 3p: three-phase short-circuit faults. [3] SLGF-LB: single-line-to-ground faults with line breaks; TPF-LB: two-phase faults with line breaks.

The distributed energy access power system disrupts the traditional one-way power flow and radial network structure of the distribution network [32]. This transformation gradually shifts the traditional distribution network from a passive mode to an active mode known as active distribution networks. Figure 1 provides an illustrative structure diagram of an active distribution network [1,32]. The aforementioned algorithms serve as a foundational framework for facilitating the extensive integration of DG into the distribution network, both in theory and technology. However, these algorithms face certain limitations, including the following: (a) weak resilience against transition resistance; (b) predominantly considering scenarios with DG penetration below 25%, which does not adequately address high-penetration DG integration; and (c) the inability to simultaneously meet the protection requirements for both short-circuit faults and disconnection faults.

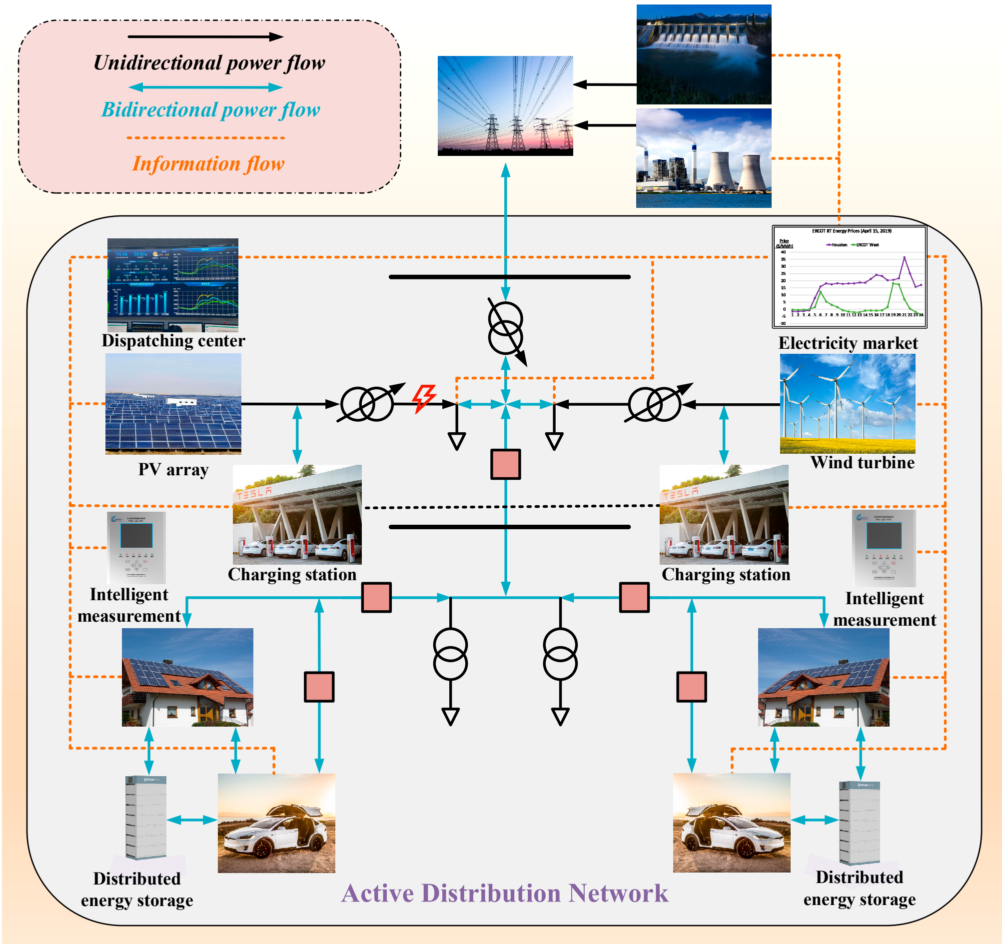

Figure 1. Structure diagram of active distribution network [1,23,32].

Hence, it becomes imperative to explore enhanced protection methodologies to address these challenges. Recognizing the advantageous characteristics of fault components, specifically their insensitivity to load states and transition resistance at fault points, as well as their high sensitivity. This paper proposes a pilot protection method for active distribution networks based on the fault component coefficient.

The proposed method leverages the ratio between the estimated and measured voltage fault components to identify internal and external faults in the line. Solely through measuring three-phase current and voltage. It caters to the protection requirements of active distribution networks in various fault scenarios, such as short-circuit and open-circuit faults, eliminating the need for fault phase identification. The method boasts advantages, including minimal susceptibility to the penetration of distributed energy sources and strong tolerance to transient resistances. Firstly, in Section 2, through the analysis of the mechanisms of short-circuit and line break faults in the distribution network, it is concluded that a disparity exists between the measured and calculated values of the voltage fault component during the fault occurrence. A method of measuring the measured value and the calculated value by using the voltage fault component is proposed. Then, using the conclusion of Section 2, the fault criterion is designed in Section 3. Fault detection is carried out via the fault mutation quantity, which improves the sensitivity of the algorithm. Finally, Section 4 verifies the correctness of the proposed algorithm by considering the simulation of short-circuit faults, line break grounded/ungrounded faults, high penetration, and transition resistance.

2. Analysis of Fault Component Characteristics of Active Distribution Network

Figure 2 presents a simplified diagram illustrating line faults in an active distribution network. In the diagram, DG represents distributed power supply, f_1 denotes the internal fault point, f_2 represents the external fault point, and Z_L denotes the line impedance. Additionally, the fault location parameter, d, is introduced to represent the distance ratio from the fault point to bus M to the total length of the feeder MN. The value range for d is [0, 1].

Distributed generation in an active distribution network can be broadly classified into two main types: motor-type distributed generators (MTDG) and inverter-interfaced distributed generators (IIDG) [23,33]. Regarding MTDG, the additional fault network can be described in Figure 3 [34].

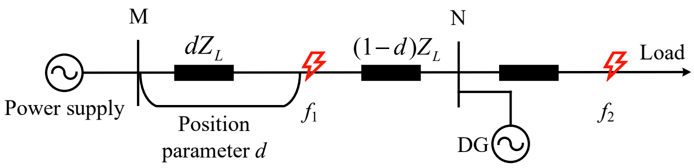

Figure 2. Simplified line fault diagram of an active distribution network [33,35,36].

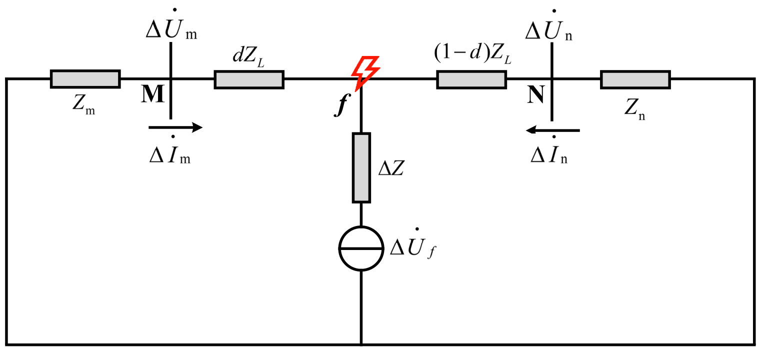

Figure 3. Distribution network of additional short-circuit fault network with MTDG.

Figure 3 shows the additional short-circuit fault network of the distribution network. The fault is located at point f; $Z_m = -(\Delta\dot{U}_m/\Delta\dot{I}_m)$ is the equivalent impedance of the M-terminal back-side system of the line, $Z_n = -(\Delta\dot{U}_n/\Delta\dot{I}_n)$ is the equSSivalent impedance of the N-terminal back-side system of the line; Z_L is the line impedance; ΔZ is the transition resistance of the fault point; $\Delta\dot{U}_f$ is the additional fault voltage source; $\Delta\dot{I}_m$ and $\Delta\dot{I}_n$ are the measured values of the current fault components at both ends; and $\Delta\dot{U}_m$ and $\Delta\dot{U}_n$ are the actual values of the voltage fault components at both ends.

As a nonlinear power supply, the output current of an IIDG undergoes abrupt changes following a fault occurrence. It is crucial to highlight that IIDG exclusively generates positive sequence current and has no impact on the negative sequence network [37,38]. Consequently, IIDG can be effectively represented as a controlled positive sequence current source [39,40]. The additional fault network for IIDG is shown in Figure 4.

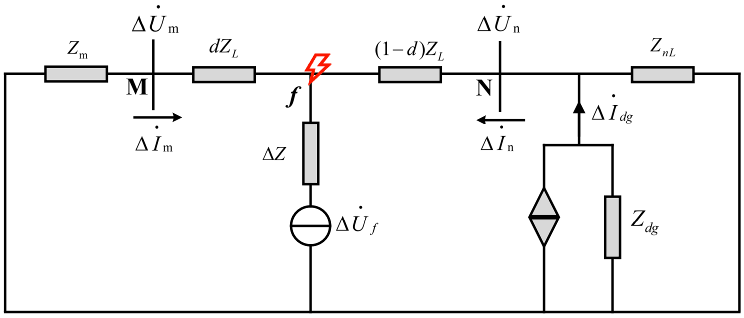

Figure 4. Distribution network of additional short-circuit fault network with IIDG [22,23].

As shown in Figure 4, Z_n is the equivalent impedance of the downstream line and load of the distributed power supply; Z_{dg} is an infinite equivalent impedance, which is used to limit the maximum short-circuit current of IIDG. $\Delta\dot{I}_{dg}$ is the current fault component of the IIDG output.

For the convenience of subsequent analysis, the additional fault network shown in Figure 5 is used. For the positive sequence additional fault network, the N-terminal back-end system is equivalent to the impedance $Z_n = -(\Delta\dot{U}_n/\Delta\dot{I}_n) = -Z_{nL}(\Delta\dot{I}_{dg} - \Delta\dot{I}_n)/\Delta\dot{I}_n = -Z_{nL}(\Delta\dot{I}_{dg}/\Delta\dot{I}_n - 1)$ that changes with the current fault component output using IIDG, and the changing impedance Z_n is used to reflect the influence of IIDG on the fault component [41]. For the negative sequence network, Z_n is a fixed impedance.

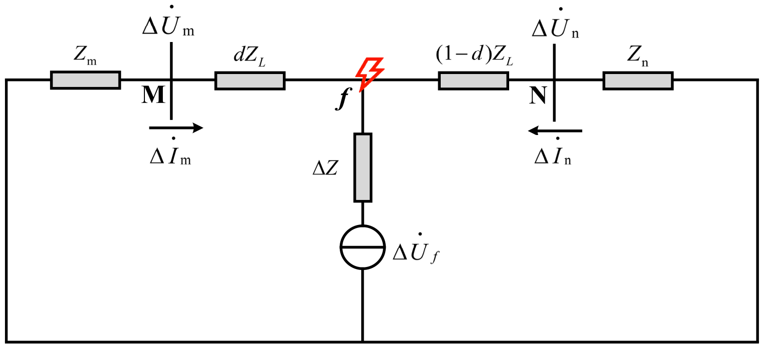

Figure 5. Simplified additional short-circuit fault network of distribution network with IIDG [36].

Similarly, the additional fault network of the distribution network with line break fault is shown in Figure 6.

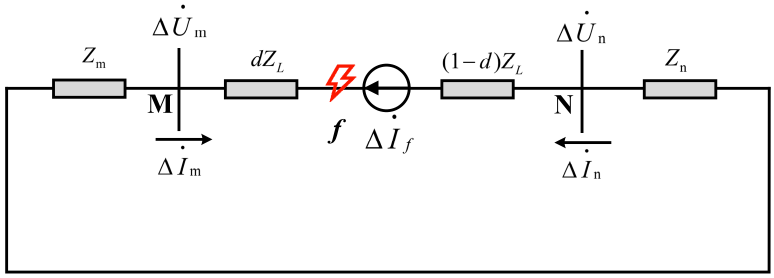

Figure 6. Distribution network with additional network of line break fault [25].

The fault point of the line break fault in the circuit shown in Figure 6 is the f point; $\Delta\dot{I}_f$ is an additional fault current source; $\Delta\dot{I}_m$ and $\Delta\dot{I}_n$ are the measured values of the current fault components at both ends; $\Delta\dot{U}_m$ and $\Delta\dot{U}_n$ are the actual values of the voltage fault components at both ends; d is the ratio of the distance from the fault point to the M-terminal to the full length of the line MN; and the value range is [0, 1].

2.1. Analysis of Short-Circuit Fault Characteristics of Active Distribution Network

Figure 7a,b depict the additional fault network for external and internal distribution line short-circuit faults, respectively. In the case of a fault occurring outside the line, the actual voltage and current fault component values can be measured at one end of the line, and the line impedance can be obtained using Ohm's law. The voltage fault component value on the opposite side of the line can be calculated using the following equation [42]:

$$\begin{bmatrix} \Delta\dot{U}_m \\ \Delta\dot{U}_n \end{bmatrix} = \begin{bmatrix} \Delta\dot{U}_n - \Delta\dot{I}_n Z_L \\ \Delta\dot{U}_m - \Delta\dot{I}_m Z_L \end{bmatrix} \quad (1)$$

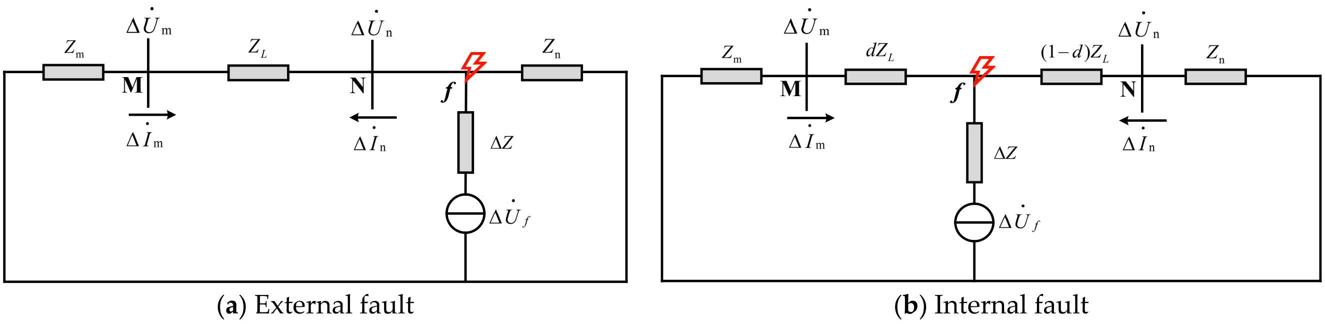

Figure 7. Additional fault network of short-circuit fault in distribution network [42,43].

Based on Equation (1), the calculation formula of the terminal voltage fault component is defined as the following:

$$\begin{bmatrix} \Delta\dot{U}'_m \\ \Delta\dot{U}'_n \end{bmatrix} = \begin{bmatrix} \Delta\dot{U}_n - \Delta\dot{I}_n Z_L \\ \Delta\dot{U}_m - \Delta\dot{I}_m Z_L \end{bmatrix} \quad (2)$$

where $\Delta\dot{U}'_m$ and $\Delta\dot{U}'_n$ are the estimated values of the voltage fault components at both ends of the line. Obviously, when an external fault occurs, the measured value of the voltage fault component at both ends of the line is consistent with the calculated value.

When an internal fault occurs in the line, the measured value of the voltage fault component at both ends of the line can be expressed using Equation (3) [23]:

$$\begin{cases} \Delta\dot{U}_m = -\Delta\dot{I}_m Z_m = \dfrac{\Delta\dot{U}_f}{\Delta Z + (Z_m + dZ_L) \| [Z_n + (1-d)Z_L]} \cdot \dfrac{Z_n + (1-d)Z_L}{Z_m + Z_n + Z_L} \cdot Z_m \\ \Delta\dot{U}_n = -\Delta\dot{I}_n Z_n = \dfrac{\Delta\dot{U}_f}{\Delta Z + (Z_m + dZ_L) \| [Z_n + (1-d)Z_L]} \cdot \dfrac{Z_n + dZ_L}{Z_m + Z_n + Z_L} \cdot Z_n \end{cases} \quad (3)$$

To assess the deviation between the calculated and actual values of the voltage fault component on both sides of the line, a comparison is conducted. This is achieved by introducing the voltage fault component ratio, as depicted in Equation (4):

$$\begin{cases} K_m = \left| \dfrac{\Delta\dot{U}'_m}{\Delta\dot{U}_m} \right| \\ K_n = \left| \dfrac{\Delta\dot{U}'_n}{\Delta\dot{U}_n} \right| \end{cases} \quad (4)$$

The ratio of voltage fault components on both sides of the line can be obtained from Equations (2)–(4), as expressed using Equation (5):

$$\begin{cases} K_m = \left|\frac{\Delta\dot{U}'_m}{\Delta\dot{U}_m}\right| = \left|\frac{Z_L+Z_n}{Z_n+(1-d)Z_L}\cdot\frac{dZ_L+Z_m}{Z_m}\right| = \left|\left(1+\frac{dZ_L}{Z_n+(1-d)Z_L}\right)\cdot\left(1+\frac{dZ_L}{Z_m}\right)\right| \\ K_n = \left|\frac{\Delta\dot{U}'_n}{\Delta\dot{U}_n}\right| = \left|\frac{Z_L+Z_m}{Z_m+(1-d)Z_L}\cdot\frac{(1-d)Z_L+Z_n}{Z_n}\right| = \left|\left(1+\frac{dZ_L}{Z_m+(1-d)Z_L}\right)\cdot\left(1+\frac{(1-d)Z_L}{Z_n}\right)\right| \end{cases} \tag{5}$$

From Equation (5), it can be seen that if a short-circuit fault occurs, regardless of the size of Z_m and Z_n, the values of K_m and K_n are greater than 1, so the change of system impedance Z_m and Z_n on both sides of the line does not affect the effectiveness of the proposed method. Therefore, the proposed method is less affected by the change in DG penetration. When d = 0, K_m is equal to 1, and K_n is greater than 1; when d = 1, K_n is equal to l, and K_m is greater than 1; when 0 < d < 1, the fault component ratio coefficients on both sides of the line are greater than l. From the above analysis, it can be concluded that the maximum value of the ratio of voltage fault components on both sides of the line is greater than l when a short-circuit fault occurs.

2.2. Analysis of Fault Characteristics of Active Distribution Network Line Break Fault

In the event of a line break fault in the distribution network, it is typical to encounter a line break grounding fault on one or both sides of the fault point. Depending on whether the power supply side or the load side is grounded, line break faults can be categorized into two cases: line break faults without grounding and line break faults accompanied by grounding. This section provides an analysis of these two types of line break faults.

2.2.1. Analysis of Ungrounded Fault Characteristics of Line Break Fault

Figure 8a,b depict the additional networks that emerge when the external and internal feeders of the distribution network experience a breakage at fault point f. $\Delta\dot{I}_f$ indicates an additional fault current source. The fault component of the terminal voltage can be calculated using Equation (2). For an external fault, the relationship between the estimated value and the actual value of the voltage fault component is elucidated using Equation (6):

$$\begin{bmatrix} \Delta\dot{U}_m \\ \Delta\dot{U}_n \end{bmatrix} = \begin{bmatrix} \Delta\dot{U}'_m \\ \Delta\dot{U}'_n \end{bmatrix} = \begin{bmatrix} \Delta\dot{U}_n - \Delta\dot{I}_n Z_L \\ \Delta\dot{U}_m - \Delta\dot{I}_m Z_L \end{bmatrix} \tag{6}$$

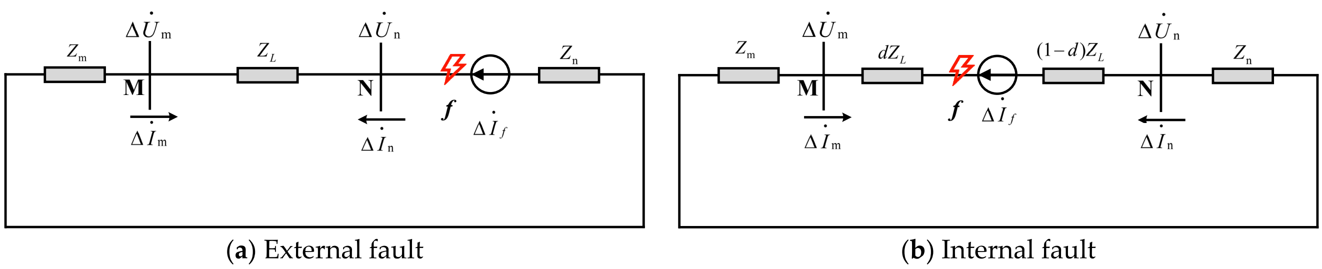

Figure 8. Additional fault network of distribution network with line break fault [26].

When an internal fault occurs, the measured value of the voltage fault component on both sides of the line is calculated as shown in Equation (7):

$$\begin{bmatrix} \Delta\dot{U}_m \\ \Delta\dot{U}_n \end{bmatrix} = \begin{bmatrix} -\Delta\dot{I}_m Z_m \\ -\Delta\dot{I}_n Z_n \end{bmatrix} = \begin{bmatrix} \Delta\dot{I}_f Z_m \\ -\Delta\dot{I}_f Z_n \end{bmatrix} \tag{7}$$

The calculated values of the voltage fault components on both sides of the line can be calculated from Equations (2)–(7), as shown in Equation (8):

$$\begin{bmatrix} \Delta\dot{U}'_m \\ \Delta\dot{U}'_n \end{bmatrix} = \begin{bmatrix} -\Delta\dot{I}_f(Z_n + Z_L) \\ \Delta\dot{I}_f(Z_n + Z_L) \end{bmatrix} \tag{8}$$

By substituting Equations (7) and (8) into Equation (4), the ratio of voltage fault components on both sides of the line can be obtained, as shown in Equation (9):

$$\begin{cases} K_m = \left| \frac{\Delta\dot{U}'_m}{\Delta\dot{U}_m} \right| = \left| \frac{Z_L + Z_n}{Z_m} \right| \\ K_n = \left| \frac{\Delta\dot{U}'_n}{\Delta\dot{U}_n} \right| = \left| \frac{Z_L + Z_m}{Z_n} \right| \end{cases} \tag{9}$$

It can be seen from Equation (9) that the change in DG penetration and the output fault component of IIDG will lead to a change in Z_n, which will affect the ratio of the voltage fault component. With the change of Z_n, there will be three impedance relationships: $Z_n > Z_m$, $Z_n = Z_m$, and $Z_n < Z_m$. The analysis is as follows:

(1) $Z_n > Z_m$, then $Z_n + Z_L > Z_m$, $K_m > 1$; K_n is affected by the values of $Z_m + Z_L$ and Z_n in the following three cases: $Z_m + Z_L > Z_n$, $K_n > 1$; $Z_m + Z_L = Z_n$, $K_n = 1$; and $Z_m + Z_L < Z_n$, $K_n < 1$. From the above analysis, the maximum value of the voltage fault component ratio on both sides of the line is greater than l.

(2) $Z_n = Z_m$, then $Z_n + Z_L > Z_m$, $K_m > 1$; $Z_m + Z_L > Z_n$, $K_n > 1$; the maximum value of the ratio of voltage fault components on both sides of the line is greater than 1.

(3) $Z_n < Z_m$, which is dual to Case (1). Similarly, the maximum value of the ratio of voltage fault components on both sides of the line is greater than 1.

In summary, the maximum value of the voltage fault component ratio on both sides of the line is also greater than 1 when the feeder is disconnected and ungrounded.

2.2.2. Analysis of the Characteristics of Line Break Fault Accompanied by Grounding Fault

When both sides of the disconnection points are grounded, the characteristics of the line break fault align with those of grounding short-circuit faults [26]. Hence, this section exclusively focuses on analyzing scenarios where grounding occurs on one side of the disconnection point.

Figure 9a,b illustrate the additional fault networks that arise when the distribution line experiences an external or internal line break fault accompanied by a ground fault on one side at fault point f. In the case of an external line break fault, the relationship between the estimated value and the actual value of the voltage fault component aligns with Equation (6). Meanwhile, for an internal fault, the measured value of the voltage fault component on both sides of the line can be expressed using Equation (10):

$$\begin{bmatrix} \Delta\dot{U}_m \\ \Delta\dot{U}_n \end{bmatrix} = \begin{bmatrix} -\Delta\dot{I}_m Z_m \\ -\Delta\dot{I}_n Z_n \end{bmatrix} = \begin{bmatrix} k\Delta\dot{I}_f Z_m \\ -\Delta\dot{I}_f Z_n \end{bmatrix} \tag{10}$$

where the coefficient k is the ratio of the M-side current $\Delta\dot{I}_m$ to the fault current source current $\Delta\dot{I}_f$, and $k = -\Delta\dot{I}_m / \Delta\dot{I}_f$.

From Equations (2)–(10), the estimated value of the voltage fault component on both sides of the line can be obtained, as shown in Equation (11):

$$\begin{bmatrix} \Delta\dot{U}'_m \\ \Delta\dot{U}'_n \end{bmatrix} = \begin{bmatrix} \Delta\dot{U}_n \\ \Delta\dot{U}_m \end{bmatrix} - \begin{bmatrix} \Delta\dot{I}_n Z_n \\ \Delta\dot{I}_m Z_m \end{bmatrix} = \begin{bmatrix} -\Delta\dot{I}_f(Z_n + Z_L) \\ k\Delta\dot{I}_f(Z_m + Z_L) \end{bmatrix} \tag{11}$$

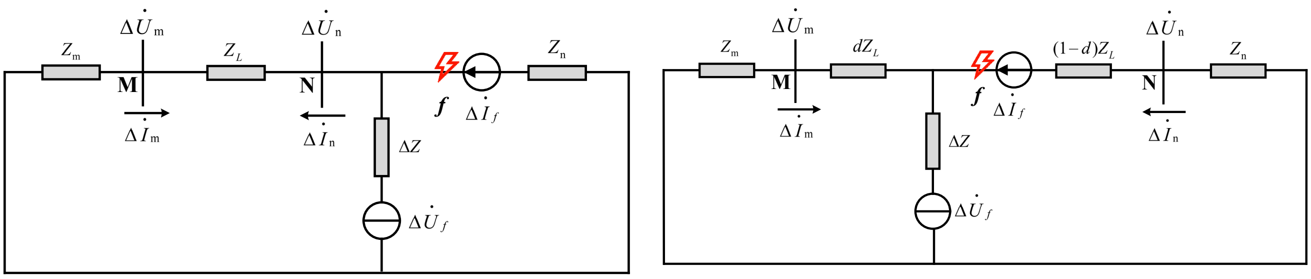

Figure 9. Distribution network line break fault with one side of the additional ground fault network [25].

Substituting Equations (10) and (11) into Equation (4), the ratio of voltage fault components on both sides can be obtained, which can be expressed using Equation (12):

$$\begin{cases} K_m = \left| \dfrac{\Delta\dot{U}'_m}{\Delta\dot{U}_m} \right| = \left| \dfrac{Z_L+Z_n}{kZ_m} \right| \\ K_n = \left| \dfrac{\Delta\dot{U}'_n}{\Delta\dot{U}_n} \right| = \left| \dfrac{k(Z_L+Z_m)}{Z_n} \right| \end{cases} \tag{12}$$

It can be seen from Equation (12) that DG penetration and coefficient k will affect the ratio of voltage fault components. With the change of DG penetration and k value, there will be three impedance relationships: $Z_n > kZ_m$, $Z_n = kZ_m$, and $Z_n < kZ_m$. The analysis is as follows:

(1) $Z_n > kZ_m$, then $Z_n + Z_L > kZ_m$, $K_m > 1$; at this time, K_n is affected by the value of $k(Z_m + Z_L)$ and Z_n in the following three cases: $k(Z_m + Z_L) > Z_n$, $K_n > 1$; $k(Z_m + Z_L) = Z_n$, $K_n = 1$; $k(Z_m + Z_L) < Z_n$, $K_n < 1$; from the above analysis, it can be concluded that in any case, the maximum value of the voltage fault component ratio on both sides of the line is greater than 1.

(2) $Z_n = kZ_m$, then $Z_n + Z_L > kZ_m$, $K_m > 1$; $k(Z_m + Z_L) > Z_n$, $K_n > 1$; the maximum value of the ratio of voltage fault components on both sides of the line is greater than 1.

(3) $Z_n < kZ_m$, then $k(Z_m + Z_L) > Z_n$, $K_n > 1$; at this time, K_m is affected by the value of $Z_n + Z_L$ and kZ_m in the following three cases: $Z_n + Z_L > kZ_m$, $K_m > 1$; $Z_n + Z_L = kZ_m$, $K_m = 1$; $Z_n + Z_L < kZ_m < kZ_m$, $K_m < 1$: The maximum value of the voltage fault component ratio on both sides of the line is greater than l.

In summary, when the distribution network breaks with one side of the ground fault, the maximum value of the voltage fault component ratio on both sides of the line is also greater than l.

3. Integrated Feeder Protection Scheme for Active Distribution Network

3.1. Design of Protection Action Criterion

Based on the aforementioned analysis, it is evident that the maximum value K_{max} of the voltage fault component ratio on both sides of the line exceeds 1 when short-circuit faults and line break faults occur within the feeder of the active distribution network. Conversely, the maximum value K_{max} of the voltage fault component ratio on both sides of the line is less than or equal to 1 in the case of external faults. Leveraging this characteristic, the fault component coefficient K_{max}, representing the maximum value of the voltage fault component ratio on both sides of the line, can serve as an action parameter for establishing the protection criterion.

The calculation formula of the voltage fault component on both sides of the line is as follows:

$$\begin{bmatrix} \Delta\dot{U}'_{m1} \\ \Delta\dot{U}'_{m2} \\ \Delta\dot{U}'_{n1} \\ \Delta\dot{U}'_{n2} \end{bmatrix} = \begin{bmatrix} \Delta\dot{U}_{n1} - \Delta\dot{I}_{n1}Z_{L1} \\ \Delta\dot{U}_{n2} - \Delta\dot{I}_{n2}Z_{L2} \\ \Delta\dot{U}_{m1} - \Delta\dot{I}_{m1}Z_{L1} \\ \Delta\dot{U}_{m2} - \Delta\dot{I}_{m2}Z_{L2} \end{bmatrix} \tag{13}$$

where $\Delta\dot{U}'_{m1}$ and $\Delta\dot{U}'_{m2}$ are the calculated values of the corresponding M-side positive sequence voltage and negative sequence voltage fault components; $\Delta\dot{U}'_{n1}$ and $\Delta\dot{U}'_{n2}$ are the estimated values of the positive sequence voltage and negative sequence voltage fault components on the N-side of the line. $\Delta\dot{U}_{m1}$ and $\Delta\dot{U}_{m2}$ are the measured values of the corresponding M-side positive sequence voltage and negative sequence voltage fault components; $\Delta\dot{U}_{n1}$ and $\Delta\dot{U}_{n2}$ are the measured values of the positive sequence voltage and negative sequence voltage fault components on the N-side of the line. $\Delta\dot{I}_{m1}$ and $\Delta\dot{I}_{m2}$ are the measured values of the positive sequence current and negative sequence current fault components at the M end of the line. $\Delta\dot{I}_{n1}$ and $\Delta\dot{I}_{n2}$ are the measured values of the corresponding N-terminal positive sequence current and negative sequence current fault components. Z_{L1} and Z_{L2} are the positive sequence equivalent impedance and negative sequence equivalent impedance of the line, respectively. Correspondingly, the fault component ratio coefficients K_{m1}, K_{n1}, K_{m2}, and K_{n2} on both sides of the line can be expressed using Equation (14):

The calculation formula for the voltage fault component on both sides of the line is as follows:

$$\begin{cases} K_{m1} = \left| \dfrac{\Delta\dot{U}'_{m1}}{\Delta\dot{U}_{m1}} \right| \\ K_{n1} = \left| \dfrac{\Delta\dot{U}'_{n1}}{\Delta\dot{U}_{n1}} \right| \end{cases} \begin{cases} K_{m2} = \left| \dfrac{\Delta\dot{U}'_{m2}}{\Delta\dot{U}_{m2}} \right| \\ K_{n2} = \left| \dfrac{\Delta\dot{U}'_{n2}}{\Delta\dot{U}_{n2}} \right| \end{cases} \tag{14}$$

The protection action criterion is shown in Formula (15):

$$\begin{cases} K_{max} = max(K_{m1}, K_{n1}, K_{m2}, K_{n2}) \\ \overline{K}_{max} = \dfrac{\sum_{n=1}^{400} K_{\max_n}}{400} > K_{set} \end{cases} \tag{15}$$

where the fault component coefficient K_{max} represents the maximum value of the fault component ratio, while $\overline{K}_{max}$ signifies the mean value of the fault component coefficient after the action. To capture the concentration trend of the fault component coefficient values in the two cycles following the fault and eliminate errors stemming from sampling synchronization and measurement, the mean value of the fault component coefficient $\overline{K}_{max}$ and K_{set} are utilized as the criteria. In the simulation, a sampling frequency of 1000 Hz is set, resulting in 400 sampling points across the two-cycle wave after 0.1 s. Each sampling point provides a fault component coefficient, K_{maxn}. K_{set} serves as the threshold value for protection action, with a theoretical value of 1. It should be noted that the sampling frequency can be adjusted based on actual conditions. The magnitude of the sampling frequency primarily impacts the smoothness of the fault component coefficient variation plot but does not affect the correctness of the criterion. When feasible, a higher frequency sampling is recommended, as it enables a more accurate reflection of the fault component ratio changes after the fault [33].

Consequently, the fault protection criterion is defined as follows: if the mean value of the voltage fault component coefficient on both sides of the line satisfies the protection criterion $\overline{K}_{max} > K_{set}$, it indicates the presence of an internal fault within the line. Conversely, when the mean value of the fault component coefficients on both sides of the line is $\overline{K}_{max} < K_{set}$, it can be judged that there is no fault in the normal operation of the line or that there is a fault outside the line.

The line parameters in the voltage fault component calculation formula are set to a fixed value, but the actual operation of the line may be affected by temperature, meteorological factors, and other conditions so that the line parameters change within the range of 10% [44,45]. The calculation formula for the terminal voltage fault component can be expressed using Equation (16):

$$\begin{bmatrix} \Delta\dot{U}'_m \\ \Delta\dot{U}'_n \end{bmatrix} = \begin{bmatrix} \Delta\dot{U}_n - \Delta\dot{I}_n Z_L \\ \Delta\dot{U}_m - \Delta\dot{I}_m Z_L \end{bmatrix} \tag{16}$$

Assuming that the line parameters change by 10%, the actual value of the terminal voltage should be the following:

$$\begin{bmatrix} \Delta\dot{U}_m \\ \Delta\dot{U}_n \end{bmatrix} = \begin{bmatrix} \Delta\dot{U}_n - 0.9\Delta\dot{I}_n Z_L \\ \Delta\dot{U}_m - 0.9\Delta\dot{I}_m Z_L \end{bmatrix} \tag{17}$$

From Equations (16) and (17), it can be seen that the ratio of voltage fault components on both sides of the line during external faults can be expressed using Equation (18):

$$\begin{cases} K_m = \left|\frac{\Delta\dot{U}'_m}{\Delta\dot{U}_m}\right| = \left|1 + \frac{0.1}{\frac{Z_n}{Z_L}+0.9}\right| \\ K_n = \left|\frac{\Delta\dot{U}'_n}{\Delta\dot{U}_n}\right| = \left|1 + \frac{0.1}{\frac{Z_m}{Z_L}+0.9}\right| \end{cases} \tag{18}$$

Because $Z_m > Z_L$, $Z_n > Z_L$ in the active distribution network, the minimum limit value of $\frac{Z_m}{Z_L}$, $\frac{Z_n}{Z_L}$ is 1, and the ratio of voltage fault component ratio fluctuates from 0 to 5.26% due to the change in line parameters. According to Equation (5), the ratio of voltage fault components on both sides of the line when the internal fault and the line parameters change is as follows.

From Equations (16) and (17), it can be seen that the ratio of voltage fault components on both sides of the line during external faults can be expressed using Equation (18):

$$\begin{cases} K_m = \left|\frac{\Delta\dot{U}'_m}{\Delta\dot{U}_m}\right| = \left|\frac{Z_L+Z_n}{Z_n+0.9(1-d)Z_L}\cdot\frac{0.9dZ_L+Z_m}{Z_m}\right| = \left|1+\frac{(0.1+0.9d)Z_L}{Z_n+0.9(1-d)Z_L}\cdot\left(1+\frac{0.9dZ_L}{Z_m}\right)\right| \\ K_n = \left|\frac{\Delta\dot{U}'_n}{\Delta\dot{U}_n}\right| = \left|\frac{Z_L+Z_m}{Z_m+0.9dZ_L}\cdot\frac{0.9(1-d)Z_L+Z_n}{Z_n}\right| = \left|1+\frac{0.1dZ_L}{Z_m+0.9dZ_L}\cdot\left(1+\frac{0.9(1-d)Z_L}{Z_n}\right)\right| \end{cases} \tag{19}$$

Taking the minimum limit value l of $\frac{Z_m}{Z_L}$, $\frac{Z_n}{Z_L}$, the fluctuation range of the voltage fault component ratio caused by the change of line parameters is 0 to 5.26%.

Therefore, considering the influence of measurement error, line parameter inaccuracies, and transient processes during the transition of the distribution network's operational state, K_{set} can be adjusted to 1.1.

3.2. Overall Process of Fault Identification

Figure 10 illustrates the comprehensive workflow of the pilot protection scheme for active distribution networks, which relies on the fault component coefficient. Initially, real-time voltage and current measurements are obtained at both ends of the line. The protection mechanism is initiated when the abrupt change in voltage and current on both sides of the circuit exceeds a predetermined threshold. To enhance the responsiveness and sensitivity of the protection startup, the criteria for phase voltage mutation and phase current mutation are utilized as triggering conditions, as depicted in Equation (20) [23,46,47]:

$$\begin{cases} ||u(t)| - |u(t-\mathrm{T})| - |u(t-\mathrm{T}) - u(t-2\mathrm{T})|| \geq 0.1U_N \\ ||i(t)| - |i(t-\mathrm{T})| - |i(t-\mathrm{T}) - i(t-2\mathrm{T})|| \geq 0.1I_N \end{cases} \quad (20)$$

where $u(t)$ represents the t-th sampling value of phase voltage, $i(t)$ represents the t-th sampling value of phase current, T represents a power frequency cycle, U_N is the rated voltage of the line, and I_N is the rated current of the line. In order to prevent the sampling data distortion caused by misoperation, only when the voltage and current of any phase in the three-phase continuous sampling points meet Formula (20) is it regarded as the mutation start.

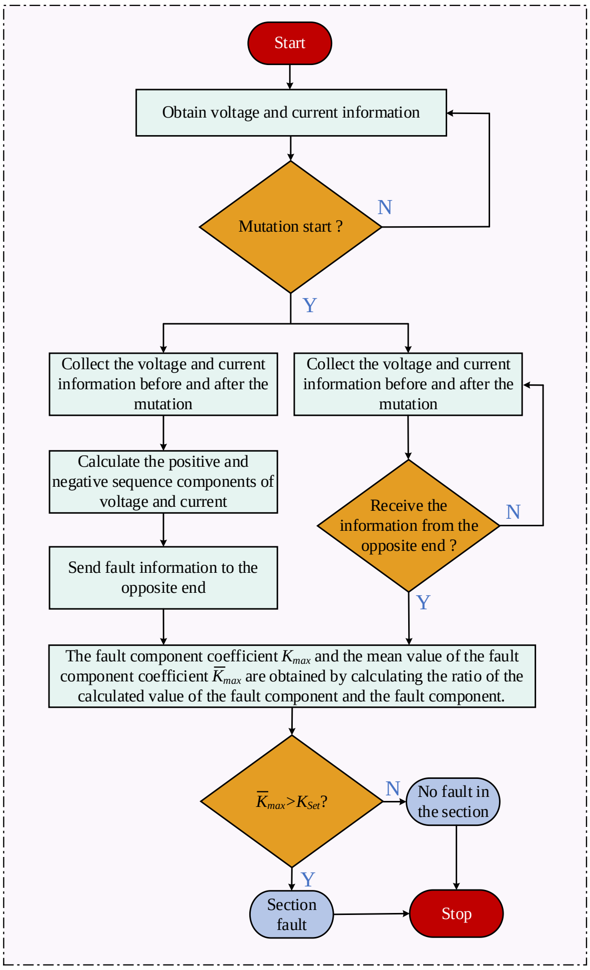

Figure 10. Flow chart of pilot protection for active distribution network based on fault component coefficient.

The current and voltage data from two cycles before and after the fault occurrence are gathered. Positive sequence and negative sequence fault components of voltage and current are obtained with the fast Fourier transform and symmetrical component method. At the same time, the fault information is sent to the opposite end, and the opposite end information is requested. Then, the protection at both ends of the line uses Equations (13) and (14) to calculate the calculated value of the voltage fault component on both sides of the line and the ratio of the voltage fault component K_{m1}, K_{n1}, K_{m2}, and K_{n2} according to the voltage and current fault information of the end and the opposite end. When the protection criterion is satisfied, the protection on both sides of the line is opened, the circuit breaker is disconnected, and the fault line is removed.

4. Simulation Experiment

4.1. Network Training Process

In order to verify the effectiveness of the proposed protection and the correctness of the analysis of the short-circuit fault and line break fault characteristics mentioned above, the Simulink simulation software(MATLAB/Simulink R2023a) is used to build a 10 kV neutral point ungrounded active distribution network model, as shown in Figure 11. The transformer capacity is 50 MVA, the transformer ratio is 35/10.5 kV, and the neutral point of the system is not grounded. Due to the tree-like multi-branch and multi-segment structure of the distribution network, the distances between sections are generally short. In this case, the longest line is only 3 km, allowing us to neglect the influence of line-to-ground capacitance. The length of line K_3–K_4 is 3 km, and the other line sections are 2 km. The line parameters are (0.27 + i0.335) Ω/km; the two DGs are MTDG and IIDG, respectively, with a rated capacity of 2.5 MW; the capacity of load L_1 is 2 MW; and the power factor is 0.9. The capacity of loads L_2 and L_3 is 0.5 MW, and the power factor is 0.9. The remaining loads are 1 MW, and the power factor is 0.9. Please refer to Table 2 for detailed simulation parameter settings.

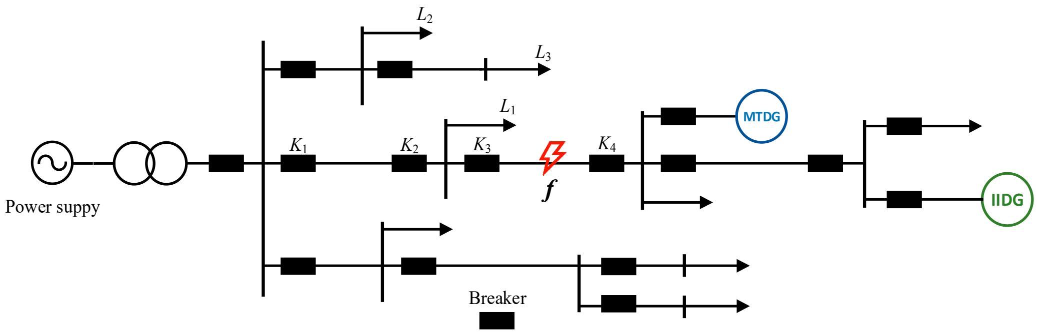

Figure 11. A 10 kV distribution line simulation model.

Table 2. Simulation parameter settings.

Parameters	Value
Voltage level	10 kV
Neutral ground mode	Neutral point ungrounded
Fault resistance	10 Ω
Transformer capacity	50 MVA
Transformer ratio	35 kV/10.5 kV
Line parameter	(0.27 + i0.335) Ω/km
Line type	Overhead
Load L_1 capacity	2 MW
Loads L_2 and L_3 capacity	0.5 MW
Line K_3–K_4 length	3 km
IIDG and MTDG capacity	2.5 MW
Load power factor	0.9
Fault occurrence time	0.1 s
Sampling frequency	1000 Hz
Simulation platform	Matlab/Simulink
Software version	Matlab R2023a
Processor model	Intel Core i5-13490F
Total cores	10
Total threads	16
Max turbo frequency	4.80 GHz

4.2. Simulation Results and Analysis

4.2.1. Short-Circuit Fault Test

Since most of the medium-voltage distribution networks in China use small current grounding (neutral point ungrounded or resonant grounding), the system can continue to operate for a short time when a single-phase grounding short-circuit fault occurs without the need to immediately remove the fault [48]. Therefore, the research conducted in this paper only focuses on phase-to-phase short circuit and two-phase ground short-circuit faults. By setting different short-circuit fault types (two-phase short circuit, two-phase ground short circuit, and three-phase short circuit) at different positions (front end, middle end, and back end) of section K_3–K_4, the simulation is carried out. Figure 12 illustrates the variation diagram of the fault component coefficient K_{max} variation diagram of the fault at section K_3–K_4 when the two-phase short-circuit fault occurs at the fault point with the position parameter d = 0.5 at 0.1 s. It could be noted that after 0.1 s, the fault component coefficient K_{max} is greater than the protection action threshold K_{set}, and the protection determines the fault.

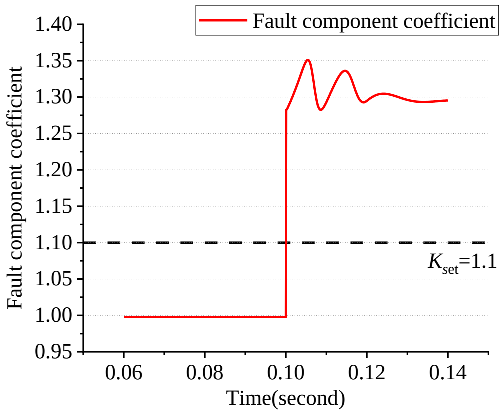

Figure 12. Variation of fault component coefficient K_{max} of K_3–K_4 in two-phase short-circuit fault section, d = 0.5.

The variation of the fault component coefficient K_{max} of the non-fault section K_1–K_2 is shown in Figure 13.

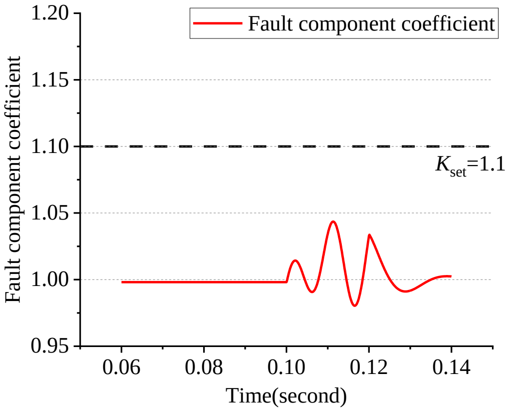

Figure 13. Variation of fault component coefficient K_{max} of non-fault section K_1–K_2, d = 0.5.

In the non-fault section K_1–K_2, the mean value of the fault component coefficient $\overline{K}_{max}$ is 1.00531852 < 1.1 within 0.1–0.14 s, and the protection determines that the line is normal and fault-free. The mean value of the fault component coefficient $\overline{K}_{max}$ of fault section K_3–K_4 in 0.1–0.14 s is 1.30553715 > 1.1, and the protection determines that the fault occurs. Table 1 shows the simulation results of the short-circuit fault scenario, indicating that the protection method can accurately identify the line short-circuit fault.

The following can be seen from Table 3: (a) Under different short-circuit fault conditions, the protection can correctly identify the fault line section. When the $\overline{K}_{max}$ is less than the threshold value when the fault occurs outside the protection area, the protection does not act; when the fault occurs in the protection area, the $\overline{K}_{max}$ is greater than the threshold value, and the protection determines the fault of the line. (b) When the fault occurs at different positions of the same fault line, $\overline{K}_{max}$ increases first and then decreases with the increase in the fault location parameter d. When the fault occurs in the middle of the line, $\overline{K}_{max}$ is the smallest, but it still meets the protection sensitivity requirements.

Table 3. Short-circuit fault simulation results.

Position Parameter d	Fault Type	Section	$\overline{K}_{max}$	Fault Identification Results
0.25	Two-phase short-circuit fault	K_1–K_2	1.00452335	Healthy
		K_3–K_4	1.43335721	Faulty
0.5	Two-phase short-circuit fault	K_1–K_2	1.00531852	Healthy
		K_3–K_4	1.30553715	Faulty
0.75	Two-phase short-circuit fault	K_1–K_2	1.00524208	Healthy
		K_3–K_4	1.48783995	Faulty
0.25	Two-phase ground short-circuit fault	K_1–K_2	1.00616038	Healthy
		K_3–K_4	1.44378926	Faulty
0.5	Two-phase ground short-circuit fault	K_1–K_2	1.00636571	Healthy
		K_3–K_4	1.28764943	Faulty
0.75	Two-phase ground short-circuit fault	K_1–K_2	1.00594443	Healthy
		K_3–K_4	1.47080818	Faulty
0.25	Three-phase short-circuit	K_1–K_2	1.02263250	Healthy
		K_3–K_4	30.18323953	Faulty
0.5	Three-phase short-circuit	K_1–K_2	1.01697544	Healthy
		K_3–K_4	25.73002623	Faulty
0.75	Three-phase short-circuit	K_1–K_2	1.01366902	Healthy
		K_3–K_4	21.68199272	Faulty

4.2.2. Line Break Fault Test

The simulation involves introducing various line break faults (single-phase line break fault and two-phase line break fault) at different positions along sections K_3–K_4. Figures 14 and 15 show the variation of the fault component coefficient K_{max} of the fault sections K_3–K_4 and the non-fault sections K_1–K_2 when the single-phase line break fault occurs at the position parameter d = 0.5 at 0.1 s. The mean value $\overline{K}_{max}$ of the K_1–K_2 fault component coefficient in the non-fault section is 0.99748631 < 1.1, which does not meet the protection criterion, and the protection determines that the line is normal without fault. The mean value $\overline{K}_{max}$ of the fault component coefficient of the fault sections K_3–K_4 is 19.63649547 > 1.1, and the protection determines that the fault occurs. Table 4 presents the simulation results for all line break fault scenarios, demonstrating the method's accuracy in pinpointing the line where a line break fault occurs.

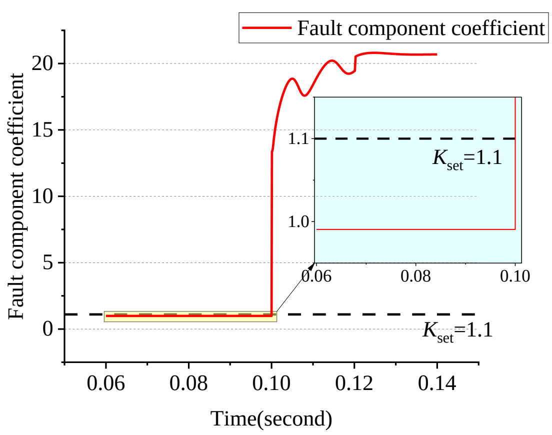

Figure 14. Variation of the fault component coefficient K_{max} of K_3–K_4 in the single-phase line break fault section, d = 0.5.

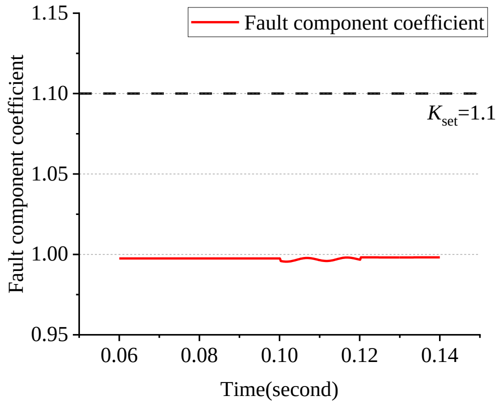

Figure 15. Variation of fault component coefficient K_{max} of non-fault section K_1–K_2, d = 0.5.

Table 4. Simulation results of line break fault.

Position Parameter d	Fault Type	Section	$\overline{K}_{max}$	Fault Identification Results
0.25	Single-phase line break fault	K_1–K_2 K_3–K_4	0.99749078 19.63702697	Healthy Faulty
0.5	Single-phase line break fault	K_1–K_2 K_3–K_4	0.99748631 19.63649547	Healthy Faulty
0.75	Single-phase line break fault	K_1–K_2 K_3–K_4	0.99749270 19.63725363	Healthy Faulty
0.25	Two-phase line break fault	K_1–K_2 K_3–K_4	0.99733227 19.70849115	Healthy Faulty
0.5	Two-phase line break fault	K_1–K_2 K_3–K_4	0.99733227 19.70849118	Healthy Faulty
0.75	Two-phase line break fault	K_1–K_2 K_3–K_4	0.99733135 19.70834086	Healthy Faulty
0.25	Single-phase line break fault	K_1–K_2 K_3–K_4	0.99749078 19.63702697	Healthy Faulty
0.5	Single-phase line break fault	K_1–K_2 K_3–K_4	0.99748631 19.63649547	Healthy Faulty
0.75	Single-phase line break fault	K_1–K_2 K_3–K_4	0.99749270 19.63725363	Healthy Faulty

From Table 4 and the above analysis, the following can be seen: (a) Under different line break faults, the proposed protection can correctly identify the fault line section. When the external fault occurs, $\overline{K}_{max}$ is less than the threshold value, and the protection does not act. When the fault occurs in the fault zone, $\overline{K}_{max}$ is much larger than the threshold value, and the protection determines the fault of the line with high sensitivity. (b) $\overline{K}_{max}$ does not change with the increase in fault location parameter d when the same fault line breaks at different locations.

4.2.3. DG Penetration Adaptability Test

Varied DG penetration levels have an impact on the equivalent impedance of the system on both sides of the line [49,50]. In order to verify the effectiveness of the protection method proposed here under different DG penetration, by changing the DG penetration in the model shown in Figure 11, a three-phase short-circuit fault is set at the position parameter d = 0.5 of K_3–K_4 lines with different DG penetrations for testing. Figures 16 and 17 are the change curves of the fault component coefficient K_{max} of lines K_3–K_4 and K_1–K_2 under different DG penetration, respectively.

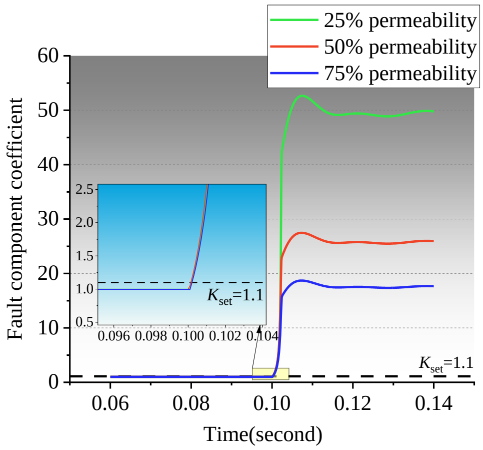

Figure 16. Variation of the fault component coefficient K_{max} of K_3–K_4 in the three-phase short-circuit fault section, d = 0.5.

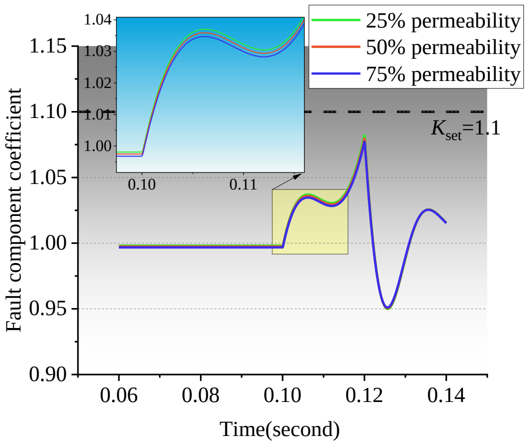

Figure 17. Variation of fault component coefficient values of non-fault section K_1–K_2, d = 0.5.

According to Figure 16, it can be seen that in the case of higher permeability, the larger the capacity of DG, the larger the fault current output of DG in case of failure, that is, the N-terminal voltage of the line is increased. This reduces the degree of voltage dip due to failure, i.e., the gap between $\Delta\dot{U}_n$ and $\Delta\dot{U}'_n$ is smaller. In the formula, the decrease in K_{max} is expressed, that is, the increase in the permeability of the system will lead to the decrease in $\overline{K}_{max}$.

Table 5 is the mean value of fault component coefficient $\overline{K}_{max}$ and fault identification results of lines K_1–K_2 and K_3–K_4 when a three-phase short-circuit fault occurs at different position parameters d of line K_3–K_4 under different DG penetration. The simulation results demonstrate that the proposed method is relatively insensitive to DG penetration. The mean value of the fault component coefficient consistently exceeds 1, allowing for accurate identification of the fault line under different DG penetration levels.

The following can be seen from Table 5: (a) Under different DG penetrations, when a three-phase short-circuit fault occurs at the same position of the line, $\overline{K}_{max}$ decreases with the increase in DG penetration. For example, when a three-phase short-circuit fault occurs at the head of the line when DG penetration is 25%, $\overline{K}_{max}$ = 58.32904694; when the DG penetration is 50%, $\overline{K}_{max}$ = 30.18323953 when the three-phase short circuit occurs at the head of the line; and when the DG penetration is 75%, $\overline{K}_{max}$ = 20.25079176 when the three-phase short circuit occurs at the head of the line. (b) With the increase in DG penetration, $\overline{K}_{max}$ has a downward trend. However, even if $\overline{K}_{max}$ becomes smaller, it still meets the protection criterion $\overline{K}_{max}$ > 1.1. Therefore, the penetration rate of distributed generation will not lead to misoperation or rejection of protection under short-circuit faults.

Table 5. Fault simulation results under different DG penetrations.

Penetration	Position Parameter d	Section	$\overline{K}_{max}$	Fault Identification Results
25%	0.25	K_1–K_2	1.02327159	Healthy
		K_3–K_4	58.32904694	Faulty
25%	0.5	K_1–K_2	1.01757253	Healthy
		K_3–K_4	49.70675315	Faulty
25%	0.75	K_1–K_2	1.01424047	Healthy
		K_3–K_4	40.47229053	Faulty
50%	0.25	K_1–K_2	1.02263250	Healthy
		K_3–K_4	30.18323953	Faulty
50%	0.5	K_1–K_2	1.01697544	Healthy
		K_3–K_4	25.73002623	Faulty
50%	0.75	K_1–K_2	1.01366902	Healthy
		K_3–K_4	21.68199272	Faulty
75%	0.25	K_1–K_2	1.02196167	Healthy
		K_3–K_4	20.25079176	Faulty
75%	0.5	K_1–K_2	1.01635410	Healthy
		K_3–K_4	17.52670797	Faulty
75%	0.75	K_1–K_2	1.01307602	Healthy
		K_3–K_4	14.14927281	Faulty

4.2.4. Line Break Fault Grounding Test

The simulation is carried out by setting different types of line break grounding faults (single-phase line break fault with power side grounding, single-phase line break fault with load side grounding, single-phase line break fault with power side and load side grounding, two-phase line break fault with power side grounding, two-phase line break fault with load side grounding, and two-phase line break fault with power side and load side grounding) at the position parameter d = 0.5 of sections K_3–K_4. Figure 18 shows the change of the fault component coefficient K_{max} of K_3–K_4 in the fault section when three single-phase line break faults occur at the position parameter d = 0.5 at 0.1 s. The mean max of the fault component coefficients of the fault section K_3–K_4 are 4.19406084, 16.48615426, and 1.28819534, respectively, which are all greater than 1.1, and the protection determines that the fault occurs. Table 6 shows the simulation results of the line break grounding fault scenario. The simulation results show that this method can correctly deal with the line break grounding fault.

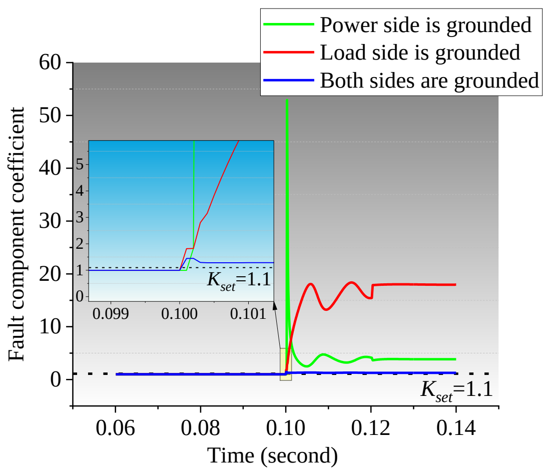

Figure 18. Variation of fault component coefficient K_{max} of K_3–K_4 in single-phase line break fault section, d = 0.5.

Table 6. Simulation results of line break grounding fault.

Fault Type	Fault Grounding Situation	Section	$\overline{K}_{max}$	Fault Identification Results
Single-phase line break fault	Power-side grounding	K_1–K_2 K_3–K_4	0.99939979 4.19406084	Healthy Faulty
Single-phase line break fault	Load-side grounding	K_1–K_2 K_3–K_4	0.99749299 16.48615426	Healthy Faulty
Single-phase line break fault	Both the power side and the load side are grounded	K_1–K_2 K_3–K_4	0.99939944 1.28819534	Healthy Faulty
Two-phase line break fault	Power-side grounding	K_1–K_2 K_3–K_4	1.00636365 1.87862998	Healthy Faulty
Two-phase line break fault	Load-side grounding	K_1–K_2 K_3–K_4	0.99733277 13.59002453	Healthy Faulty
Two-phase line break fault	Both the power side and the load side are grounded	K_1–K_2 K_3–K_4	1.00636316 1.28863630	Healthy Faulty

Based on the analysis presented in Table 6, it is evident that the proposed protection method accurately identifies the fault line section under various complex line break fault conditions. When the $\overline{K}_{max}$ is less than the threshold value when the fault occurs outside the protection area, the protection does not act; when the fault occurs in the protection area, $\overline{K}_{max}$ is greater than the threshold value, and the protection determines the fault of the line with high sensitivity.

4.2.5. Resistance to Transition Resistance Test

In the fault simulation of transition resistance, faults are set at different positions of lines K_3–K_4 for testing, and the fault type is a two-phase grounding short circuit. Figure 19 shows the change of the fault component coefficient K_{max} of K_3–K_4 in the fault section when the two-phase grounding short-circuit fault occurs at the position parameter d = 0.5 at 0.1 s. The mean $\overline{K}_{max}$ of K_3–K_4 fault component coefficients in the fault section are 1.28764943, 1.28781090, and 1.28781841, respectively, and the protection determines that the fault occurs. Table 7 shows the mean value of fault component coefficient $\overline{K}_{max}$ and fault determination results of lines K_3–K_4 under different transition resistances. The simulation results indicate that the proposed method is minimally impacted by transition resistance and can accurately identify faults even in high-resistance fault scenarios.

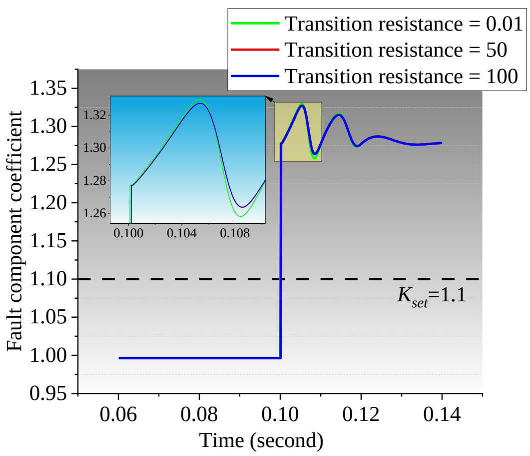

Figure 19. Variation of the fault component coefficient K_{max} of K_3–K_4 in the two-phase ground short-circuit fault section, d = 0.5.

Table 7. Fault simulation results under different transition resistances.

Transition Resistance (Ω)	Position Parameter d	Section	$\overline{K}_{max}$	Fault Identification Results
0.01	0.25	K_1–K_2	1.00616038	Healthy
		K_3–K_4	1.44178926	Faulty
0.01	0.5	K_1–K_2	1.00636571	Healthy
		K_3–K_4	1.28764943	Faulty
0.01	0.75	K_1–K_2	1.00594443	Healthy
		K_3–K_4	1.47080818	Faulty
50	0.25	K_1–K_2	1.00527347	Healthy
		K_3–K_4	1.44269517	Faulty
50	0.5	K_1–K_2	1.00571027	Healthy
		K_3–K_4	1.28781090	Faulty
50	0.75	K_1–K_2	1.00542349	Healthy
		K_3–K_4	1.47105170	Faulty
100	0.25	K_1–K_2	1.00512056	Healthy
		K_3–K_4	1.44365996	Faulty
100	0.5	K_1–K_2	1.00560816	Healthy
		K_3–K_4	1.28781841	Faulty
100	0.75	K_1–K_2	1.00535039	Healthy
		K_3–K_4	1.47106406	Faulty

It can be seen from Table 7 that in the case of different transition resistances, $\overline{K}_{max}$ increases with the increase in transition resistance when a two-phase ground short-circuit fault occurs at the same position of the line. For example, when the transition resistance is 0.1 Ω, $\overline{K}_{max}$ = 1.44178926, when the two-phase grounding short circuit occurs at the front end of the line; when the transition resistance is 50 Ω, $\overline{K}_{max}$ = 1.44269517, when the two-phase ground short circuit occurs at the front end of the line; and when the transition resistance is 100 Ω, $\overline{K}_{max}$ = 1.44365996, when the two-phase ground short circuit occurs at the front end of the line. With the increase in transition resistance, the sensitivity of protection increases.

4.2.6. Protection Reliability Test When DG Has No Output When Fault Occurs

Due to the fluctuation of DG output, DG may be exactly without output or out of operation during the fault [51]. To assess the impact of DG's absence or shutdown on the proposed protection method, various fault types (two-phase short circuit and single-phase line break fault) are simulated at different positions along sections K_3–K_4 for simulation, and DG exits when a fault occurs. Figure 20 shows the change of the fault component coefficient K_{max} of K_3–K_4 in the fault section when the two-phase short-circuit fault occurs at the position parameters d = 0.25, 0.5, and 0.75 at 0.1 s. The mean $\overline{K}_{max}$ of the fault component coefficients of the fault sections K_3–K_4 are 1.42195343, 1.32007979, and 1.50114944, which are all greater than 1.1, and the protection determines that the fault occurs. Table 8 shows the simulation results for each fault scenario. The simulation results show that the proposed protection scheme can still well identify the fault that DG happens to have no output or exits from the operation.

It can be seen from Table 8 that the change trend of $\overline{K}_{max}$ with the position parameter d is basically unchanged from the above simulation results. When the DG is out of operation during the fault, it will lead to the increase in $\overline{K}_{max}$, that is, the difference between the calculated value and the measured value of the voltage fault component becomes larger, which increases the sensitivity of the protection strategy.

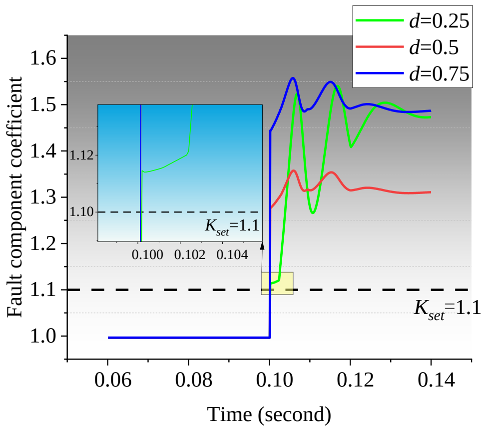

Figure 20. Variation of fault component coefficient K_{max} of K_3–K_4 in two-phase short-circuit fault section.

Table 8. Simulation results of DG out of operation when fault occurs.

Fault Type	Position Parameter *d*	Section	$\overline{K}_{max}$	Fault Identification Results
Two-phase short-circuit fault	0.25	K_1–K_2	1.00329193	Healthy
		K_3–K_4	1.42195343	Faulty
Two-phase short-circuit fault	0.5	K_1–K_2	1.00428989	Healthy
		K_3–K_4	1.32007979	Faulty
Two-phase short-circuit fault	0.75	K_1–K_2	1.00433046	Healthy
		K_3–K_4	1.50114944	Faulty
Three-phase short-circuit fault	0.25	K_1–K_2	1.02263261	Healthy
		K_3–K_4	423.57270072	Faulty
Three-phase short-circuit fault	0.5	K_1–K_2	1.01697540	Healthy
		K_3–K_4	286.70814715	Faulty
Three-phase short-circuit fault	0.75	K_1–K_2	1.01366891	Healthy
		K_3–K_4	148.15551296	Faulty
Single-phase line break fault	0.25	K_1–K_2	0.99775849	Healthy
		K_3–K_4	34.47421420	Faulty
Single-phase line break fault	0.5	K_1–K_2	0.99776118	Healthy
		K_3–K_4	34.47838064	Faulty
Single-phase line break fault	0.75	K_1–K_2	0.99775669	Healthy
		K_3–K_4	34.47143423	Faulty

5. Conclusions and Future Work

With large-scale intermittent new energy grid-connected power generation, the active distribution network plays a pivotal role in harnessing renewable energy and enhancing user power consumption reliability. The active distribution network, featuring high penetration of DG, is poised to become the primary configuration of future distribution networks. In recent years, the world has witnessed a series of blackouts triggered with HILP extreme events. These events have resulted in substantial economic and societal losses while significantly jeopardizing the power supply reliability of distribution networks. These catastrophic faults, induced by disasters, differ from conventional faults considered in traditional protection schemes. The probability of line break faults in distribution networks increases considerably during such events. Traditional protection mechanisms struggle to address this challenge, leading to a significant surge in operational risks for active distribution networks during extreme events. Consequently, in order to enhance the power supply reliability of active distribution networks under disaster scenarios, this study explores the feeder protection method tailored to catastrophic faults caused by disasters. The main research focus and conclusions are outlined as follows:

(1) The fault additional network analysis models for MTDG and IIDG are established. A detailed analysis is conducted on the characteristics of voltage fault components.

This analysis specifically focuses on the occurrence of short-circuit faults and line break faults in active distribution networks. It takes into consideration the specific fault characteristics of catastrophic faults caused by disasters. The occurrence of different fault types in the feeder leads to changes in the line topology. This results in discrepancies between the measured voltage fault component values at the protection installation points on both ends of the line and the calculated values obtained from the corresponding formulas;

(2) A novel active distribution network feeder protection method based on voltage fault components is proposed. The method takes into account the discrepancy between the calculated and measured values of the voltage fault component at both ends of the line. The proposed method utilizes the voltage fault component calculation formula, along with the measured voltage fault component and current fault component at one end of the line, to estimate the voltage fault component at the other end of the line. By comparing the calculated and measured voltage fault components, the ratio of the voltage fault component is obtained. This ratio is then utilized to identify internal and external faults in the line, effectively addressing the protection requirements of the active distribution network in various fault scenarios, including short-circuit faults and line break faults. Finally, a simulation model of the active distribution network is developed using the Matlab/Simulink R2023a to validate the reliability and effectiveness of the proposed protection scheme. However, under the HILP events, the distribution network protection should not only deal with the single fault but also deal with the complex fault. In this paper, the complex fault is not analyzed and studied. In the future, the adaptability of the protection proposed in this paper under multiple repeated faults will be further analyzed to improve the shortcomings and construct a more perfect active distribution network protection criterion.

Author Contributions: Conceptualization, L.X. and S.F.; methodology, H.Z.; software, J.X.; validation, C.L.; formal analysis, L.X.; writing—review and editing, S.M. All authors have read and agreed to the published version of the manuscript.

Funding: This work was supported by the Science and Technology Project of State Grid Corporation of China (Research and application of fusion perception, intelligent diagnosis and service enhancement technologies at the end of rural power network) under grant No. 52199922000M.

Data Availability Statement: Not applicable.

Conflicts of Interest: The authors declare no conflict of interest.

Nomenclature

Symbols and abbreviations	
DG	Distributed generation
HILP	High impact and low probability
ADNs	Active distribution networks
WTRP	Wireless token ring protocol
DT	Distribution transformer
TPFs-LBs	Two-phase faults with line breaks
TPFs-SCs	Two-phase short-circuit faults
SLGFs-LBs	Single-line-to-ground faults with line breaks
SLGFs	Single-line-to-ground faults
MTDG	Motor-type distributed generators
IIDG	Inverter-interfaced distributed generators
d	Fault location parameter
Z_L	Line impedance
Z_m	Equivalent impedance of the M-terminal back-side system of the line
Z_n	Equivalent impedance of the N-terminal back-side system of the line
ΔZ	Transition resistance of the fault point
ΔU_f	Fault additional voltage source

ΔI_m, ΔI_n	Measured values of the current fault components at both ends
ΔU_m, ΔU_n	Actual values of the voltage fault components at both ends
Z_{dg}	Infinite equivalent impedance
ΔI_{dg}	Current fault component of the IIDG output
K_{max}	Fault component coefficient
K_{max}	Mean value of the fault component coefficient
ΔI_f	Additional fault current source
$\Delta U'_m$, $\Delta U'_n$	Estimated values of the voltage fault components at both ends
k	Ratio of the ΔI_m to ΔI_f
$\Delta U'_{m1}$, $\Delta U'_{m2}$	M-side positive and negative sequence voltage fault components
$\Delta U'_{n1}$, $\Delta U'_{n2}$	N-side positive and negative sequence voltage fault components
Z_{L1}, Z_{L2}	Positive and negative sequence equivalent impedance
K_{set}	Threshold value for protection action
$u(t)$	The t-th sampling value of phase voltage
T	Power frequency cycle
U_{N}	Rated voltage
I_{N}	Rated current
$i(t)$	The t-th sampling value of phase current

References

1. Mishra, D.K.; Ghadi, M.J.; Azizivahed, A.; Li, L.; Zhang, J. A review on resilience studies in active distribution systems. *Renew. Sustain. Energy Rev.* **2021**, *135*, 110201. [CrossRef]
2. Xie, J.; Jin, G.; Wang, Y.; Ni, X.; Liu, X. New Algorithm for 2-terminal Transmission Line Fault Location Integrating Voltage Phasor Feature and Phase Angle Jump Checking. *Electr. Power Syst. Res.* **2022**, *209*, 107971. [CrossRef]
3. Wang, Y.; Rousis, A.O.; Strbac, G. On microgrids and resilience: A comprehensive review on modeling and operational strategies. *Renew. Sustain. Energy Rev.* **2020**, *134*, 110313. [CrossRef]
4. Macmillan, M.; Murphy, C.A.; Bazilian, M.D. Exploring acute weather resilience: Meeting resilience and renewable goals. *Renew. Sustain. Energy Rev.* **2022**, *168*, 112841. [CrossRef]
5. Jia, Y.; Liu, Y.; Wang, B.; Lu, D.; Lin, Y. Power Network Fault Location with Exact Distributed Parameter Line Model and Sparse Estimation. *Electr. Power Syst. Res.* **2022**, *212*, 108137. [CrossRef]
6. Li, T.; Li, Y.; Chen, X.; Li, S.; Zhang, W. Research on AC Microgrid with Current-Limiting Ability Using Power-State Equation and Improved Lyapunov-Function Method. *IEEE J. Emerg. Sel. Top. Power Electron.* **2021**, *9*, 7306–7319. [CrossRef]
7. Coleman, N.; Esmalian, A.; Lee, C.-C.; Gonzales, E.; Koirala, P.; Mostafavi, A. Energy inequality in climate hazards: Empirical evidence of social and spatial disparities in managed and hazard-induced power outages. *Sustain. Cities Soc.* **2023**, *92*, 104491. [CrossRef]
8. Younesi, A.; Shayeghi, H.; Wang, Z.; Siano, P.; Mehrizi-Sani, A.; Safari, A. Trends in modern power systems resilience: State-of-the-art review. *Renew. Sustain. Energy Rev.* **2022**, *162*, 112397. [CrossRef]
9. Yao, Y.; Liu, W.; Jain, R.; Chowdhury, B.; Wang, J.; Cox, R. Quantitative Metrics for Grid Resilience Evaluation and Optimization. *IEEE Trans. Sustain. Energy* **2023**, *14*, 1244–1258. [CrossRef]
10. Jufri, F.H.; Widiputra, V.; Jung, J. State-of-the-art review on power grid resilience to extreme weather events: Definitions, frameworks, quantitative assessment methodologies, and enhancement strategies. *Appl. Energy* **2019**, *239*, 1049–1065. [CrossRef]
11. Ti, B.; Li, G.; Zhou, M.; Wang, J. Resilience Assessment and Improvement for Cyber-Physical Power Systems under Typhoon Disasters. *IEEE Trans. Smart Grid* **2022**, *13*, 783–794. [CrossRef]
12. Xie, H.; Sun, X.; Chen, C.; Bie, Z.; Catalao, J.P.S. Resilience Metrics for Integrated Power and Natural Gas Systems. *IEEE Trans. Smart Grid* **2022**, *13*, 2483–2486. [CrossRef]
13. Quijano, D.A.; Padilha-Feltrin, A. Optimal integration of distributed generation and conservation voltage reduction in active distribution networks. *Int. J. Electr. Power Energy Syst.* **2019**, *113*, 197–207. [CrossRef]
14. Dehghani, F.; Mohammadi, M.; Karimi, M. Age-dependent resilience assessment and quantification of distribution systems under extreme weather events. *Int. J. Electr. Power Energy Syst.* **2023**, *150*, 109089. [CrossRef]
15. Grajales-Espinal, C.; Mora-Florez, J.; Perez-Londono, S. Advanced fault location strategy for modern power distribution systems based on phase and sequence components and the minimum fault reactance concept. *Electr. Power Syst. Res.* **2016**, *140*, 933–941. [CrossRef]
16. Liu, J.; Qin, C.; Yu, Y. A Comprehensive Resilience-Oriented FLISR Method for Distribution Systems. *IEEE Trans. Smart Grid* **2021**, *12*, 2136–2152. [CrossRef]
17. Zeineldin, H.H.; Sharaf, H.M.; Ibrahim, D.K.; El-Zahab, E.E.-D.A. Optimal protection coordination for meshed distribution systems with DG using dual setting directional over-current relays. *IEEE Trans. Smart Grid* **2015**, *6*, 115–123. [CrossRef]
18. Chilvers, I.; Jenkins, N.; Crossley, P.A. Distance relaying of 11 kV circuits to increase the installed capacity of distributed generation. *Gener. Transm. Distrib. IEE Proc.* **2005**, *152*, 40–46. [CrossRef]

19. Jalilian, A.; Hagh, M.T.; Hashemi, S.M. An innovative directional relaying scheme based on postfault current. *IEEE Trans. Power Deliv.* **2014**, *29*, 2640–2647. [CrossRef]
20. Xyngi, I.; Popov, M. An intelligent algorithm for the protection of smart power systems. *IEEE Trans. Smart Grid* **2013**, *4*, 1541–1548. [CrossRef]
21. Eissa, M.M. Protection technique for complex distribution smart grid using wireless token ring protocol. *IEEE Trans. Smart Grid* **2012**, *3*, 1106–1118. [CrossRef]
22. Nsengiyaremye, J.; Pal, B.C.; Begovic, M.M. Microgrid Protection Using Low-Cost Communication Systems. *IEEE Trans. Power Deliv.* **2020**, *35*, 2011–2020. [CrossRef]
23. Gao, H.; Li, J.; Xu, B. Principle and implementation of current differential protection in distribution networks with high penetration of DGs. *IEEE Trans. Power Deliv.* **2017**, *32*, 565–574. [CrossRef]
24. Avendano-Mora, M.; Milanović, J.V. Generalized formulation of the optimal monitor placement problem for fault location. *Electr. Power Syst. Res.* **2012**, *93*, 120–126. [CrossRef]
25. Li, H.; Xue, Y.; Chen, M.; Zhang, Z. Analysis of Voltage Characteristics for Single-Phase Line Break Fault in Resonant Grounding Systems. *IEEE Trans. Power Deliv.* **2023**, *38*, 1416–1425. [CrossRef]
26. Zichang, L.; Yadong, L.; Yingjie, Y.; Peng, W.; Xiuchen, J. An Identification Method for Asymmetric Faults with Line Breaks Based on Low-Voltage Side Data in Distribution Networks. *IEEE Trans. Power Deliv.* **2021**, *36*, 3629–3639. [CrossRef]
27. Liang, Y.; Lu, Z.; Li, W.; Zha, W.; Huo, Y. A Novel fault impedance calculation method for distance protection against fault resistance. *IEEE Trans. Power Deliv.* **2020**, *35*, 396–407. [CrossRef]
28. Ghorbani, A.; Sanaye-Pasand, M.; Mehrjerdi, H. Accelerated distance protection for transmission lines based on accurate fault location. *Electr. Power Syst. Res.* **2021**, *193*, 107021. [CrossRef]
29. Mohanty, R.; Sahoo, S.; Pradhan, A.K.; Blaabjerg, F. A cosine similarity-based centralized protection scheme for dc microgrids. *IEEE J. Emerg. Sel. Top. Power Electron.* **2021**, *9*, 5646–5656. [CrossRef]
30. Liu, Y.; Li, Z.; Yan, Y.; He, G.; Fang, J.; Li, K.; Jiang, X. Identification Method for Single-line-to-ground Faults with Line Break Based on Phasor Measurement in Distribution Networks. *J. Mod. Power Syst. Clean Energy* **2023**, *11*, 907–916. [CrossRef]
31. Zhou, N.; Han, B.; Xu, Y.; Luo, L.; Sheng, G.; Jiang, X. Fault locating and severity assessment for power distribution systems based on elasticity network topology mapping. *Int. J. Electr. Power Energy Syst.* **2023**, *144*, 108570. [CrossRef]
32. Cho, N.; Yun, S.; Jung, J. Determining the reverse fault current by the type of transformer and Distributed Generation in distribution system during the single-line to ground fault. *Renew. Sustain. Energy Rev.* **2019**, *109*, 102–115. [CrossRef]
33. Zang, L.; Zou, G.; Zhou, C.; Zheng, M.; Du, T. A d-axis based current differential protection scheme for an active distribution network. *Prot. Control Mod. Power Syst.* **2022**, *7*, 23. [CrossRef]
34. Hsieh, T.-Y.; Chen, T.-H.; Yang, N.-C.; Lee, W.-J. Efficient network fault analysis method for unbalanced microgrid systems. *Int. J. Electr. Power Energy Syst.* **2018**, *103*, 89–101. [CrossRef]
35. Yu, C.; Gao, Z.; Liu, Z.; Tao, Z. Current Differential Protection for Active Distribution Networks Based on Adaptive Phase Angle Compensation Coefficient. *Appl. Sci.* **2023**, *13*, 4723. [CrossRef]
36. Miao, X.; Zhao, D.; Lin, B.; Jiang, H.; Chen, J. A Differential Protection Scheme Based on Improved DTW Algorithm for Distribution Networks With Highly-Penetrated Distributed Generation. *IEEE Access* **2023**, *11*, 40399–40411. [CrossRef]
37. Li, Y.; Wang, D. Asymmetrical fault analysis on distribution feeders with inverter interfaced distributed generators. *Int. J. Electr. Power Energy Syst.* **2021**, *125*, 106514. [CrossRef]
38. Baran, M.E.; El-Markaby, I. Fault analysis on distribution feeders with distributed generators. *IEEE Trans. Power Syst.* **2005**, *20*, 1757–1764. [CrossRef]
39. Yuan, J.; Hu, Y.; Liang, Y.; Jiao, Z. Faulty Feeder Detection for Single Line-to-Ground Fault in Distribution Networks with DGs Based on Correlation Analysis and Harmonics Energy. *IEEE Trans. Power Deliv.* **2023**, *38*, 1020–1029. [CrossRef]
40. Guo, W.-M.; Mu, L.-H.; Zhang, X. Fault Models of Inverter-Interfaced Distributed Generators Within a Low-Voltage Microgrid. *IEEE Trans. Power Deliv.* **2017**, *32*, 453–461. [CrossRef]
41. Eskandari, M.; Savkin, A.V. On the Impact of Fault Ride-Through on Transient Stability of Autonomous Microgrids: Nonlinear Analysis and Solution. *IEEE Trans. Smart Grid* **2021**, *12*, 999–1010. [CrossRef]
42. Ansari, S.; Gupta, O.H.; Kumar, S. A novel protection scheme for microgrid feeders using differential positive sequence apparent power features. *Electr. Eng.* **2023**, *105*, 2971–2985. [CrossRef]
43. Ansari, S.; Gupta, O.H. Differential Negative Sequence Power Angle-Based Protection of Microgrid Feeders. *Electr. Power Compon. Syst.* **2022**, *49*, 1417–1431. [CrossRef]
44. Yu, J.; Weng, Y.; Rajagopal, R. Patopaem: A data-driven parameter and topology joint estimation framework for time-varying system in distribution grids. *IEEE Trans. Power Syst.* **2019**, *34*, 1682–1692. [CrossRef]
45. Mirshekali, H.; Dashti, R.; Shaker, H.R.; Samsami, R.; Torabi, A.J. Linear and Nonlinear Fault Location in Smart Distribution Network under Line Parameter Uncertainty. *IEEE Trans. Ind. Inform.* **2021**, *17*, 8308–8318. [CrossRef]
46. Zhou, C.; Zou, G.; Zhang, S.; Zheng, M.; Tian, J.; Du, T. Mathematical Morphology-Based Fault Data Self-Synchronization Method for Differential Protection in Distribution Networks. *IEEE Trans. Smart Grid* **2022**, *14*, 2607–2620. [CrossRef]
47. Zhou, C.; Zou, G.; Du, X.; Zang, L. Adaptive current differential protection for active distribution network considering time synchronization error. *Int. J. Electr. Power Energy Syst.* **2022**, *140*, 108085. [CrossRef]

48. Wang, Q.; Jin, T.; Mohamed, M.; Deb, D. A Novel Linear Optimization Method for Section Location of Single-Phase Ground Faults in Neutral Noneffectively Grounded Systems. *IEEE Trans. Instrum. Meas.* **2021**, *70*, 3513410. [CrossRef]
49. Sharma, N.K.; Samantaray, S.R. PMU Assisted Integrated Impedance Angle-Based Microgrid Protection Scheme. *IEEE Trans. Power Deliv.* **2020**, *35*, 183–193. [CrossRef]
50. Rahman, M.T.; Hasan, K.N.; Sokolowski, P. Assessment of Conservation Voltage Reduction Capabilities Using Load Modelling in Renewable-Rich Power Systems. *IEEE Trans. Power Syst.* **2021**, *36*, 3751–3761. [CrossRef]
51. Liang, X. Emerging Power Quality Challenges Due to Integration of Renewable Energy Sources. *IEEE Trans. Ind. Appl.* **2017**, *53*, 855–866. [CrossRef]